

Redox-Active Complexes Containing Group 8 Metal Centers Linked by C₂ Bridges

Michael I. Bruce,^{*,†} Karine Costuas,[‡] Ben G. Ellis,[†] Jean-François Halet,^{*,‡} Paul J. Low,^{*,§} Boujemaa Moubaraki,[⊥] Keith S. Murray,[⊥] Nadia Ouddai,^{‡,||} Gary J. Perkins,[†] Brian W. Skelton,[#] and Allan H. White[#]

Department of Chemistry, University of Adelaide, Adelaide, South Australia 5005, Laboratoire des Sciences Chimiques de Rennes, UMR 6226 CNRS-Université de Rennes 1, F-35042 Rennes Cedex, France, Department of Chemistry, University of Durham, South Road, Durham DH1 3LE, England, School of Chemistry, Monash University, Clayton, Victoria 3800, Australia, Département de Chimie, Université de Batna, Rue Boukhrouf, 05000 Batna, Algeria, and Chemistry M313, SBBCS, University of Western Australia, Crawley, Western Australia 6009

Received March 25, 2007

A series of complexes containing dicarbon ligands bridging redox-active group 8 metal–ligand fragments M(dppe)Cp' (M = Fe, Ru, Os; Cp' = Cp, Cp*) have been prepared. These complexes give up to four one-electron anodic processes at a platinum electrode, with separations of successive oxidation potentials of ca. 850 mV, giving rise to large comproportionation constants, K_C (ca. 10¹²). Examples of the 36-electron neutral, 35-electron monocationic, and 34-electron dicationic species, together with some related monoprotated complexes, have been isolated. Structural studies of the 36-, 35-, and 34-electron species derived from the dicarbon complex featuring two Ru(dppe)Cp end-caps (**7**) show that shortening of the M–C and lengthening of the C–C bonds occur upon oxidation. A complementary spectroelectrochemical investigation has revealed an intense band near 14 300 cm⁻¹ associated with [7]PF₆, which is tentatively attributed to a Ru(d)–[Ru(d)/C₂(π)]* transition, rather than a genuine IVCT band. These observations have been rationalized using DFT calculations and collectively indicate that the frontier orbitals are delocalized over both group 8 metal centers and the carbon chain.

Introduction

Complexes containing redox-active metal–ligand groups linked by carbon chains continue to elicit attention, not only because of their inherent interest as metal-supported fragments of the linear carbon allotrope carbyne but also because of their possible involvement in nanoscale devices as, or as models for, molecular wires.^{1–5} The chemistry of complexes of the type {L_nM}–C_n–{ML_n} and their heterometallic analogues has recently been reviewed, and the relative paucity of compounds containing C₂ units end-capped by redox-active groups is notable.⁶

Some of us have recently examined the range of reported complexes of the type {L_nM}–CC–{ML_n} and have commented on the wide variety of electron counts and geometries.⁷ Examples where ML_n = ScCp*₂,⁸ Sm(thf)Cp*₂,⁹ Ti(PMe₃)Cp₂,¹⁰

[V(mes)₃]⁻,¹¹ Cr(CO)₃Cp,¹² Mn(CO)₅,¹³ and Fe(CO)₂Cp*¹⁴ are known for the first-row transition elements of groups 3–8, while complexes containing third-row transition metals include those with ML_n = Re(CO)₅,¹⁵ trans-PtCl(PPh₃)₂,¹⁶ Au(PR₃)₃,¹⁷ and HgMe.¹⁸ None of these have significant redox properties that might enable a comparison to be made with compounds containing longer carbon chains, such as {L_nM}–CC–CC–{ML_n}, where ML_n = Re(NO)(PPh₃)Cp*¹⁹ or M(PP)Cp' [M =

(9) Evans, W. J.; Rabe, G. W.; Ziller, J. W. *J. Organomet. Chem.* **1994**, *483*, 21.

(10) Binger, P.; Müller, P.; Phillips, P.; Gabor, B.; Mynott, R.; Herrmann, A. T.; Langhauser, F.; Krüger, C. *Chem. Ber.* **1992**, *125*, 2209.

(11) Kreisel, G.; Scholz, P.; Seidel, W. *Z. Anorg. Allg. Chem.* **1980**, *460*, 51.

(12) Ustynyuk, N. A.; Vinogradova, V. N.; Kravtsov, D. N. *Metallog. Khim.* **1988**, *1*, 85.

(13) Davies, J. A.; El-Ghanem, M.; Pinkerton, A. A.; Smith, D. A. *J. Organomet. Chem.* **1991**, *409*, 367.

(14) Akita, M.; Terada, M.; Oyama, S.; Moro-oka, Y. *Organometallics* **1990**, *9*, 816. (b) Akita, M.; Terada, M.; Oyama, S.; Sugimoto, S.; Moro-oka, Y. *Organometallics* **1991**, *10*, 1561. (c) Akita, M.; Chung, M.-C.; Sakurai, A.; Sugimoto, S.; Terada, M.; Tanaka, M.; Moro-oka, Y. *Organometallics* **1997**, *16*, 4882.

(15) Appel, M.; Heidrich, J.; Beck, W. *Chem. Ber.* **1987**, *120*, 1087.

(16) Sunkel, K.; Birk, U.; Robl, C. *Organometallics* **1994**, *13*, 1679.

(17) (a) R = Me, Et: Liau, R.-Y.; Schier, A.; Schmidbaur, H. *Organometallics* **2003**, *22*, 3199. (b) R = Ph, m-tol: Bruce, M. I.; Grundy, K. R.; Liddell, M. J.; Snow, M. R.; Tiekink, E. R. T. *J. Organomet. Chem.* **1988**, *344*, C49. (c) R = Cy: Che, C.-M.; Chao, H.-Y.; Miskowski, V. M.; Li, Y.; Cheung, K.-K. *J. Am. Chem. Soc.* **2001**, *123*, 4985.

(18) Spair, R. J.; Vogt, R. R.; Nieuwland, J. A. *J. Am. Chem. Soc.* **1933**, *55*, 2465.

(19) (a) Zhou, Y.; Seyler, J. W.; Weng, W.; Artif, A. M.; Gladysz, J. A. *J. Am. Chem. Soc.* **1993**, *115*, 8509. (b) Brady, M.; Weng, W.; Zhou, Y.; Seyler, J. W.; Amoroso, A. J.; Arif, A. M.; Böhme, M.; Frenking, G.; Gladysz, J. A. *J. Am. Chem. Soc.* **1997**, *119*, 775.

* Corresponding authors. E-mail: michael.bruce@adelaide.edu.au; halet@univ-rennes1.fr; p.j.low@durham.ac.uk.

† University of Adelaide.

‡ UMR 6226 CNRS-Université de Rennes 1.

§ University of Durham.

⊥ Monash University.

|| Université de Batna.

University of Western Australia.

(1) Ward, M. D. *Chem. Soc. Rev.* **1995**, *24*, 121.

(2) Harriman, A.; Ziessel, R. *Coord. Chem. Rev.* **1998**, *171*, 331.

(3) Paul, F.; Lapinte, C. *Coord. Chem. Rev.* **1998**, *178–180*, 431.

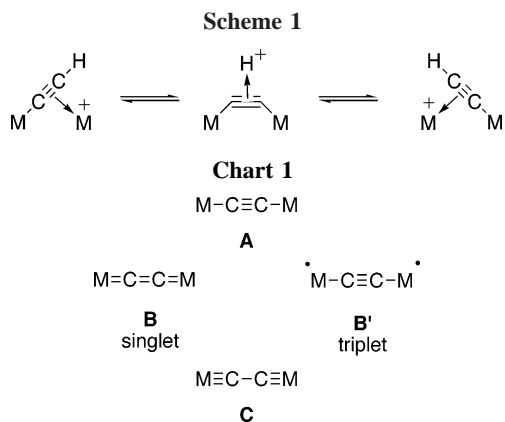
(4) Tour, J. M. *Acc. Chem. Res.* **2000**, *33*, 791.

(5) Low, P. J. *Dalton Trans.* **2005**, 2821.

(6) Bruce, M. I.; Low, P. J. *Adv. Organomet. Chem.* **2004**, *50*, 179.

(7) Ouddai, N.; Costuas, K.; Bencharif, M.; Saillard, J.-Y.; Halet, J.-F. *C. R. Chim.* **2005**, *8*, 1336.

(8) St Clair, M.; Schaefer, W. P.; Bercaw, J. E. *Organometallics* **1991**, *10*, 525.



Fe, Ru, Os; PP = (PPh₃)₂, dppe; Cp' = Cp, Cp*],^{20–22} for example. Recently, this gap was partially filled by the report describing the dicarbon complexes [Cp'(dmpe)Mn]-CC-[Mn(dmpe)Cp']ⁿ⁺ (Cp' = Cp^{Me}, n = 0–2).²³

Group 8 complexes containing ethynediyl ligands are limited to {M(CO)₂Cp'}₂(μ-C≡C) (M = Fe, Cp' = Cp*, η⁵-C₅Me₄Et; M = Ru, Cp' = Cp, Cp^{Me}). The iron complex was prepared by the reaction of Fe(C≡CH)(CO)₂Cp' with [Fe(thf)(CO)₂Cp']⁺, followed by deprotonation (NaOMe or NEt₃) of the resulting cationic product [{Fe(CO)₂Cp'}₂(μ-η¹:η²-CCH)]⁺.¹⁴ The ruthenium derivatives were obtained by metathesis of Ru(C≡CMe)(CO)Cp' with (Bu^tO)₃W≡W(OBu^t)₃.²⁴ Treatment of the ruthenium ethynediyl with HBF₄ afforded [{Ru(CO)₂Cp'}₂(μ-η¹:η²-CCH)]⁺.²⁵ The cationic complexes [{Fe(CO)₂Cp'}₂(μ-η¹:η²-CCH)]⁺ showed fluxional behavior, which has been interpreted in terms of interconversion of the bonding modes of the μ-η¹:η²-CCH ligand via a symmetrical intermediate (Scheme 1); similar processes are likely in the case of the ruthenium analogues²⁵ and related species such as [{Re(CO)₅}₂(μ-η¹:η²-CCH)]⁺.¹⁵

Interest in systems containing μ-η¹:η²-C₂ ligands is enhanced by their flexible electronic structures, which in appropriate cases encompass the three representations **A**, **B**, and **C** (Chart 1).²⁶ In valence bond terms, these may be described as the ynediyl, bis-carbene or metallacumulene, and bis-carbyne forms, respectively. Diradical species, such as the triplet **B'**, can also be written. Extensive spectroscopic, electrochemical, and structural studies of the manganese complexes mentioned above established that the neutral complex exhibits a singlet/triplet spin equilibrium (**B/B'**) at room temperature in both solution and the solid state.²³ Complementary DFT calculations on these systems, which support the low singlet–triplet energy gap, were also reported.²³

Our interest in homo- and heterometallic compounds containing group 8 metal centers has resulted in the preparation of an

extensive series of C₄ complexes^{21,27} and several derivatives containing longer carbon chains.²⁸ This interest has also caused us to examine the possibility of making the analogous, electron-rich and redox-active C₂ complexes. We noted that the complex [Cp(Ph₃P)₂Ru](μ-CN){Ru(PPh₃)₂Cp}]⁺, with redox-active group 8 metal–ligand groups end-capping the CN bridge, had been first successfully prepared and structurally characterized some 20 years ago,²⁹ with a second structural determination of this cation being reported recently.³⁰ We chose to use redox-active end-caps similar to those employed earlier, both in the CN chemistry and in our earlier studies of C₄ complexes, i.e., M(dppe)Cp' [M = Fe, Ru, Os; Cp' = Cp, Cp*], which, in the case of the ruthenium examples, gave complexes exhibiting up to four sequential one-electron oxidations.^{21c,27} However, it should be noted that these groups are bulky enough to result in steric interactions between the phenyl groups of the phosphine ligands that may impede rotation of the metal–ligand moieties about the M–C–M axis, leading on one occasion to the isolation of two rotamers of {Ru(PPh₃)₂Cp'}₂(μ-C₄) when this complex was crystallized from different solvents.^{21b} Conformational factors have been noted as playing a significant role in the electronic structures of other dicarbon species.²³

This paper reports the syntheses and structural and spectroscopic characterization of several complexes of the type [Cp'(PP)M]-CC-[M(PP)Cp']ⁿ⁺ (M = Fe, Ru, Os; PP = dppe, Cp' = Cp, Cp*; n = 0–2), together with a theoretical study using DFT methods.

Results and Discussion

The ethynediyl complexes were prepared by the sequence of reactions shown in Scheme 2. The vinylidene complexes [M(=C=CH₂)(dppe)Cp']PF₆ [Cp' = Cp, M = Fe (**1**), Ru (**2**), Os (**3**); Cp' = Cp*, M = Os (**4**)] were prepared from reactions between HC≡CSiMe₃ and the corresponding chloro complexes, MCl(dppe)Cp, carried out in Bu^tOH in the presence of [NH₄]⁺PF₆⁻ (Scheme 2). The use of Bu^tOH as solvent for these reactions avoids conversion to the alkoxy-carbene cations that occurs rapidly in primary alcohols such as MeOH or EtOH.³¹ Deprotonation of cationic vinylidene ligands occurs readily to give acetylide complexes, while deprotonation of terminal acetylides such as Re(C≡CH)(PPh₃)(NO)Cp*³² and Ru(C≡CH)(PPh₃)₂-Cp³³ with alkyl lithiums has been shown to give nucleophilic metal acetylide anions. Similar acetylide anions have also been

(20) (a) Le Narvor, N.; Lapinte, C. *J. Chem. Soc., Chem. Commun.* **1993**, 357. (b) Le Narvor, N.; Toupet, L.; Lapinte, C. *J. Am. Chem. Soc.* **1995**, *117*, 7129.

(21) (a) Bruce, M. I.; Hinterding, P.; Tiekink, E. R. T.; Skelton, B. W.; White, A. H. *J. Organomet. Chem.* **1993**, *450*, 209. (b) Bruce, M. I.; Hall, B. C.; Kelly, B. D.; Low, P. J.; Skelton, B. W.; White, A. H. *J. Chem. Soc., Dalton Trans.* **1999**, 3719. (c) Bruce, M. I.; Low, P. J.; Costuas, K.; Halet, J.-F.; Best, S. P.; Heath, G. A. *J. Am. Chem. Soc.* **2000**, *122*, 1949.

(22) Bruce, M. I.; Kramarczuk, K. A.; Perkins, G. J.; Skelton, B. W.; White, A. H. Unpublished work.

(23) Kheradmandan, S.; Venkatean, K.; Blacque, O.; Schmalke, H. W.; Berke, H. *Chem.–Eur. J.* **2004**, *10*, 4872.

(24) Koutsantonis, G. A.; Selegue, J. P. *J. Am. Chem. Soc.* **1991**, *113*, 2316.

(25) Griffith, C. S.; Koutsantonis, G. A.; Skelton, B. W.; White, A. H. *J. Organomet. Chem.* **2003**, *670*, 198.

(26) Chisholm, M. H. *Angew. Chem., Int. Ed.* **1991**, *30*, 673.

(27) (a) Bruce, M. I.; Ellis, B. G.; Low, P. J.; Skelton, B. W.; White, A. H. *Organometallics* **2003**, *22*, 3184. (b) Bruce, M. I.; Costuas, K.; Davin, T.; Ellis, B. G.; Halet, J.-F.; Lapinte, C.; Low, P. J.; Smith, M. E.; Skelton, B. W.; Toupet, L.; White, A. H. *Organometallics* **2005**, *24*, 3864.

(28) (a) Bruce, M. I.; Kramarczuk, K. A.; Zaitseva, N. N.; Skelton, B. W.; White, A. H. *J. Organomet. Chem.* **2005**, *690*, 1549. (b) Bruce, M. I.; Humphrey, P. A.; Melino, G.; Skelton, B. W.; White, A. H.; Zaitseva, N. N. *Inorg. Chim. Acta* **2005**, *358*, 1453. (c) Antonova, A. B.; Bruce, M. I.; Ellis, B. G.; Gaudio, M.; Humphrey, P. A.; Jevric, M.; Melino, G.; Nicholson, B. K.; Perkins, G. J.; Skelton, B. W.; White, A. H.; Zaitseva, N. N. *Chem. Commun.* **2004**, 960. (d) Bruce, M. I.; Kelly, B. D.; Skelton, B. W.; White, A. H. *J. Organomet. Chem.* **2000**, *604*, 150.

(29) Baird, G. J.; Davies, S. J.; Moon, S. D.; Simpson, S. J.; Jones, R. H. *J. Chem. Soc., Dalton Trans.* **1985**, 1479.

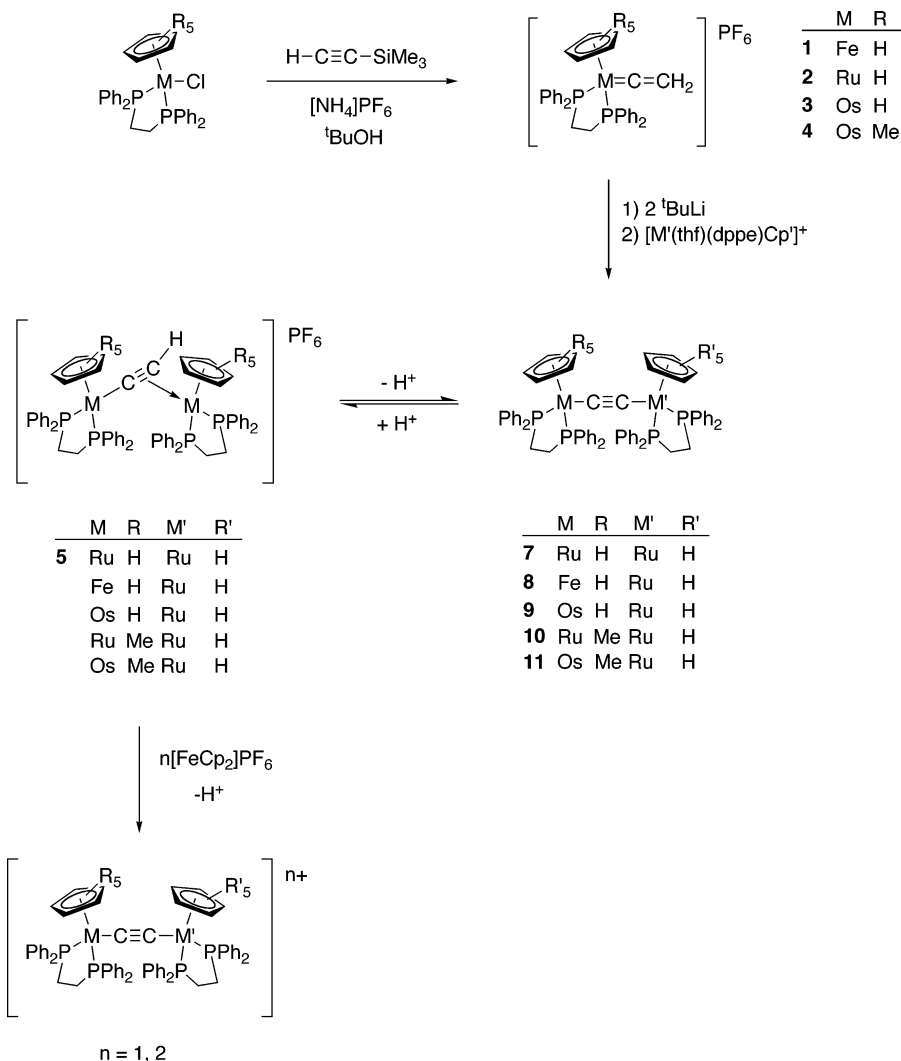
(30) Ornelas, C.; Gandum, C.; Mesquita, J.; Rodrigues, J.; Garcia, M. H.; Lopes, N.; Robalo, M. P.; Näntinen, K.; Rissanen, K. *Inorg. Chim. Acta* **2005**, *358*, 2482.

(31) Bruce, M. I.; Koutsantonis, G. A. *Aust. J. Chem.* **1991**, *44*, 207.

(32) (a) Weng, W.; Arif, A. M.; Gladysz, J. A. *Angew. Chem., Int. Ed. Engl.* **1993**, *32*, 891. (b) Ramsden, J. A.; Weng, W.; Gladysz, J. A. *Organometallics* **1992**, *11*, 3635. (c) Ramsden, J. A.; Weng, W.; Arif, A. M.; Gladysz, J. A. *J. Am. Chem. Soc.* **1992**, *114*, 5890.

(33) Cordiner, R. L.; Corcoran, D.; Yufit, D. S.; Goeta, A. E.; Howard, J. A. K.; Low, P. J. *Dalton Trans.* **2003**, 3541.

Scheme 2



obtained from reaction of $\text{Fe}(\text{C}\equiv\text{CSiMe}_3)(\text{dippe})\text{Cp}$ with MeLi^{34} or from reaction of $[\text{Ru}(\text{C}=\text{CH}_2)(\text{PPh}_3)_2\text{Cp}^*]\text{PF}_6$ or $[\text{Ru}(\text{C}=\text{CH}_2)(\text{dippe})\text{Cp}^*]\text{PF}_6$ with ≥ 2 equiv of *tert*- or *n*-BuLi.³⁵ Double deprotonation of **1–4** with 2 equiv of LiBu^t in thf gave intermediates assumed to be $\text{M}(\text{C}\equiv\text{CLi})(\text{dippe})\text{Cp}'$, which, when added to solutions of $[\text{Ru}(\text{thf})(\text{dippe})\text{Cp}]^+$ prepared *in situ* from AgOTf and $\text{RuCl}(\text{dippe})\text{Cp}$, afforded presumably the μ -ynediyl complexes **7–11**, but which were readily protonated to give the corresponding μ -ethynyl complexes $[\{\text{Cp}(\text{dippe})\text{Ru}\}(\mu-\eta^1:\eta^2\text{-CCH})\{\text{M}(\text{dippe})\text{Cp}'\}]\text{PF}_6$ [$\text{Cp}' = \text{Cp}$, $\text{M} = \text{Fe}$, **5**], Os ; $\text{Cp}' = \text{Cp}^*$, $\text{M} = \text{Fe}$ (**6a**), Ru (**6b**), Os (**6c**)] after conventional workup. As described below, most of these μ -ethynyl complexes were obtained in sufficiently high purity to be used in further reactions without further purification (Scheme 2). However, a representative sample of forest-green $[\{\text{Ru}(\text{dippe})\text{Cp}\}_2(\mu\text{-CCH})]\text{PF}_6$ (**5**) has been characterized by elemental analysis and spectroscopic methods. Thus, the ^1H NMR spectrum of **5** contains single Cp and CH resonances at δ 4.75 and 2.51, respectively, the latter showing a quintet $J(\text{HP})$ coupling, which suggests that the two ruthenium-containing fragments are equivalent in the NMR time scale and indicates that the $\mu-\eta^1:\eta^2\text{-CCH}$ group exchanges rapidly between the two metal centers.

(34) Smith, M. E.; Cordiner, R. L.; Albesa-Jové, D.; Yufit, D. S.; Hartl, F.; Howard, J. A. K.; Low, P. J. *Can. J. Chem.* **2006**, *84*, 154.

(35) (a) Kawata, Y.; Sato, M.; *Organometallics*, **1997**, *16*, 1093. (b) Cordiner, R. L.; Smith, M. E.; Batsanov, A. S.; Albesa-Jové, D.; Hartl, F.; Howard, J. A. K.; Low, P. J. *Inorg. Chim. Acta* **2006**, *359*, 946.

Although we have not yet been able to confirm the solid-state structure, analogous complexes containing $\text{M}(\text{CO})_2\text{Cp}'$ ($\text{M} = \text{Fe}$, Ru ; $\text{Cp}' = \text{Cp}$, Cp^*) end-caps are known.^{14,24}

Deprotonation of **5** with KOBU^t affords orange neutral $\{\text{Ru}(\text{dippe})\text{Cp}\}_2(\mu\text{-C}_2)$ (**7**), which was obtained in disappointingly low yields (ca. 25%). The low yield is likely a consequence of the strong basicity of **7**, which results in regeneration of **5** by reaction with protic solvents or traces of water during workup. The remarkably high basicity of $\text{Ru}(\text{C}\equiv\text{CBu}^t)(\text{PMe}_3)_2\text{Cp}$ (the $\text{p}K_a$ of $[\text{Ru}(\text{C}\equiv\text{CHBu}^t)(\text{PMe}_3)_2\text{Cp}]^+$ is 20.8 in MeCN; cf. $\text{p}K_a$ of $[\text{NHEt}_3]^+$ 18.5) had been noted before.³⁶ The NMR spectra of **7** contain a singlet at δ_{H} 4.59, assigned to two equivalent Cp groups and a broad resonance at δ_{P} 87.8 from the dppe ligands. In the ^{13}C NMR spectrum of **7**, resonances for the C_2 bridge atoms were not found as a result of poor solubility of this complex in aprotic solvents. However, the molecular structure was confirmed by a single-crystal X-ray study, the results of which are discussed below.

Treatment of cation **5** with 1 or 2 equiv of $[\text{FeCp}_2]\text{PF}_6$ results in both oxidation and deprotonation, affording deep blue $[\{\text{Ru}(\text{dippe})\text{Cp}\}_2(\mu\text{-C}_2)]\text{PF}_6$ (**7**)⁺ or magenta $[\{\text{Ru}(\text{dippe})\text{Cp}\}_2(\mu\text{-C}_2)]\text{PF}_6$ (**7**)²⁺ according to stoichiometry. We have found that the tendency toward oxidation of **7** and its congeners is so great that the dicationic species are preferred for storage, ready conversion to the monocation or neutral species being achieved

(36) Bullock, R. M. *J. Am. Chem. Soc.* **1987**, *109*, 8087.

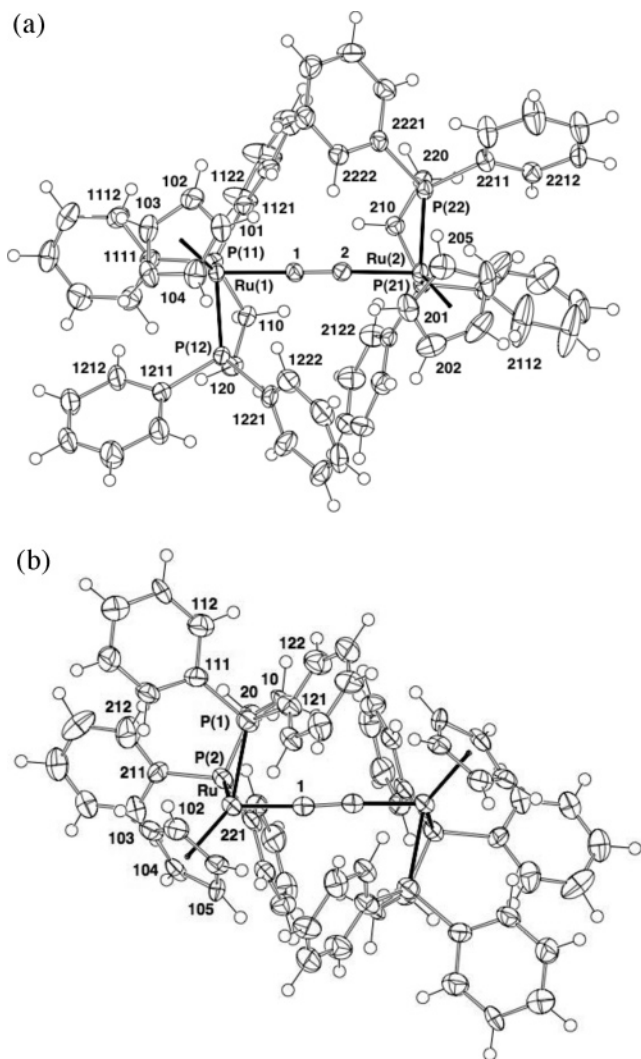


Figure 1. Representative binuclear arrays: (a) molecule of **7** [for which the Cp(0)–Ru···Ru–Cp(0) torsion is ca. 60°]; (b) cation of **[7](PF₆)₂** [for which the torsion is ca. 120°].

by treatment with KOBu^t. The mechanistic pathway of this reaction is far from clear.

Analogous reactions between 2 equiv of [FeCp₂]PF₆ and the appropriate cations [{Cp(dppe)Ru}(μ-η¹:η²-CCH){M(dppe)-Cp'}]⁺, generated *in situ*, have given [{Cp(dppe)Ru}(μ-C₂){M(dppe)Cp'}](PF₆)₂ [Cp' = Cp, M = Fe (**[8]**)²⁺, Ru (**[7]**)²⁺ (*vide supra*), Os (**[9]**)²⁺]; Cp' = Cp*, M = Ru (**[10]**)²⁺, Os (**[11]**)²⁺]. The dicationic complexes derived from **7–11** are obtained as pink or magenta solids, which exhibited ν(CC) absorptions between 1645 and 1711 cm⁻¹, and doubly charged M²⁺ ions were observed by electrospray ionization mass spectrometry.

X-ray Structural Studies. Crystallographic structure determinations of reasonable precision have been successfully carried out with a dichloromethane solvate of **7** and water and acetone solvates of **[7](PF₆)₂**. The determination on **[7]PF₆**, also reported here, is of lower precision. In all cases one formula unit, devoid of crystallographic symmetry with respect to the complex component, comprises the asymmetric unit, although in **[7]PF₆** a pair of anions are each disposed on crystallographic inversion centers. The complexes comprise arrays in which the torsions of the Cp centroids about the Ru···Ru line are either ca. 60° (in the neutral form, **7**·CH₂Cl₂) or ca. 120° in the remainder (Figure 1). The arrays are generally devoid of disorder except for minor solvent components (see below), with no unusual

features in the lattices except where some partitioning into columns or sheets occurs.

The geometries of the complex system cores are presented in Table 1. However, the difficulties of obtaining particularly precise structure determinations for the majority of materials crystallized [e.g., that of **[7](PF₆)₂** as diverse (solvated) forms, all inauspicious] naturally limit the conclusions that can be drawn directly regarding the various valence-bond descriptions depicted in Chart 1. Nevertheless, with respect to the species in the body of Table 1, Ru–P distances are shortest for neutral **7**, maximal for **[7]**⁺ and intermediate for **[7]**²⁺ with the Ru–Cp(centroid) distances displaying a similar trend. The gross Ru···Ru dimensions of the RuC₂Ru strings are similar for **7** and **[7]**⁺ and diminished by ca. 0.2 Å for the H₂O and Me₂CO solvates of **[7](PF₆)₂**.

For the neutral complex **7** (Figure 1), two Ru(dppe)Cp groups are linked by the C₂ fragment, with the torsion angle α between the two Ru···C(0) vectors [C(0) is the midpoint of the Cp ring] along the RuC₂Ru chain being 59.3°. The phenyl groups of the dppe ligands are interleaved, with evidence for π–π stacking between some of the Ph rings. The Ru–C(1,2) and C(1)–C(2) distances are 2.046(5), 2.051(5), and 1.230(7) Å, respectively, with angles at C(1,2) being 174.0(4)° and 170.2(4)°. The four Ru–P distances fall between 2.234(1) and 2.243(1) Å (av 2.237 Å). In the corresponding monocation **[7]**⁺, the Ru–C(1,2) distances are 2.00(3) and 2.02(3) Å, C(1)–C(2) lengthening to 1.28(4) Å, with angles at C(1,2) similar to those in neutral **7**. Lengthening of the Ru–P distances to between 2.317 and 2.329(10) Å is found (av 2.321 Å). The dication **[7]**²⁺ has essentially the same geometry regardless of the nature of the solvate, with Ru–C(1,2) distances of 1.878(8) and 1.881(8) Å, C(1)–C(2) distances of 1.30(1) Å, and angles at C(1,2) being 172.6(7)° and 175.6(6)°, respectively (values for acetone solvate given). The Ru–P bond distances are between 2.287(3) and 2.315(3) Å (av 2.298(11) Å). The torsion angles C(0)···Ru···C(0) range between 59.6° and 127.5° and reflect the significant steric congestion brought about by the close proximity of the two organoruthenium groups.

The Ru–C distances diminish monotonically on passing from **7** to **[7]**⁺ to **[7]**²⁺, the C–C distance increasing, consistent with a change from ethynediyl structure **A** (–Ru–C≡C–Ru–) toward the cumulenyl structure **B** (–Ru=C=C=Ru–) as oxidation proceeds; the value for the C–C distance for **[7]**⁺ is so imprecise as to be of little value. Table 1 also compares the geometric parameters of the M–CC–M systems in **7**, **[7]**⁺, and **[7]**²⁺ with those of the Mn complexes [{Mn(dmpe)Cp^{Me}}]₂(μ-C₂)ⁿ⁺ (n = 0–2), and with a similar gradual shortening of the M–C bond and lengthening of the C–C bond found as oxidation proceeds. The change from the ethynediyl structure **A** [–M–C≡C–M–] toward the cumulenyl structure **B** [–M=C=C–M–] (Chart 1) is supported by theoretical calculations.

Electronic Structure Calculations. In order better to understand some of the experimental results, a theoretical investigation was conducted at the DFT level, initially on the model systems [{Ru(dHpe)Cp}]₂(μ-C₂)ⁿ⁺, **[7-H]**ⁿ⁺ (n = 0–2, dHpe = PH₂CH₂CH₂PH₂), which were used to mimic [{Ru(dppe)Cp}]₂(μ-C₂)ⁿ⁺, **[7]**ⁿ⁺. Optimized distances and angles computed for the neutral and cationic models compare rather well with available experimental data (pertinent data can be found in Table S1 of the Supporting Information). The experimentally observed changes in the Ru–C and C–C distances that occur upon oxidation of **7** and that are supported by calculations on **[7]**ⁿ⁺ and **[7-H]**ⁿ⁺ can be rationalized by the nodal properties of the two nearly degenerate HOMOs (highest occupied molecular

Cp fragment relative to the other in the neutral model complex **7-H** has a negligible influence on the electronic and structural features of the metal–carbon core under investigation. The same conclusion is reached for the dicationic high-spin (HS) [**7-H**]²⁺ species. A very flat potential energy surface is computed with a very shallow minimum found for a C(0)···Ru···C(0) torsion angle α of 62°. Again, the energy difference between the different conformers is computed as less than 1 kJ/mol. Similar observations were made for the triplet state of model complex [**7-H**]²⁺, i.e., a very flat potential energy curve with energy minima ($\alpha = 90^\circ$ and 270°) and maximum ($\alpha = 0^\circ$) separated by less than 5 kJ/mol.²³

In contrast, the energies of the low-spin (LS) [**7-H**]²⁺ dication and, to a lesser extent, the monocation [**7-H**]⁺ are much more dependent upon the adopted conformation. For instance, in the case of (LS) [**7-H**]²⁺ a maximum energy difference of 20 kJ/mol is calculated between the most stable rotamer ($\alpha = 2^\circ$) and the least stable one ($\alpha = 56^\circ$). An even higher energy difference, ca. 36 kJ/mol, was found for the LS complex [**7-H**]²⁺. In the case of the manganese system the most stable conformer was computed for $\alpha = 180^\circ$ (*transoid* geometry) and the least stable for $\alpha = 90^\circ$ (*gauche* geometry).²³ The energy dependence upon the conformation in these M₂C₂ complexes (M = Mn or Ru) is attributed to the fact that the shape and the metal character of the two π -type fragment orbitals (FO) of the pseudo-octahedral {M(dHpe)Cp}⁺ fragment are not fully equivalent.⁷ Consequently the HOMOs of the complexes in which these FOs are involved are not degenerate but energetically slightly separated in the *transoid* geometry (Figure 2). On the other hand, they become nearly degenerate in the *gauche* geometry with some energy stabilization of the HOMO and some destabilization of the HOMO–1. If both orbitals are doubly [Ru, neutral] or singly [Mn HS (triplet) neutral; Ru, HS dication] occupied, the total energy is hardly affected by changes of conformation. On the other hand, if one is doubly occupied and one vacant [Mn LS (singlet) neutral; Ru LS dication] or partially filled [Ru monocation], the *transoid* configuration becomes more stable.

Overall, the singlet and triplet states of the dicationic Ru₂C₂ species [**7-H**]²⁺ are very close in energy, and DFT calculations carried out at the B3LYP level of theory show the triplet states (HS, $\alpha = 92^\circ$) slightly favored over the singlet states (LS, $\alpha = 2^\circ$) by only 3 kJ/mol. This is an interesting result, which strongly contrasts with the situation for dicationic diruthenium complexes containing longer carbon chain spacers such as [**12-H**]²⁺, which are diamagnetic^{27a} and for which larger singlet–triplet energy gaps have been calculated using model systems.^{21c} The relative stability of the triplet (HS) configuration in the ruthenium ethynediyl complexes is similar to the situation encountered in paramagnetic di-iron polycarbon-bridged complexes^{27b,37} and is attributed to the high metal character of the “magnetic” orbitals in [**7-H**]²⁺. In fact, the HOMO and LUMO of (LS) [**7-H**]²⁺ (which are derived from the HOMO–1 and HOMO in the neutral system) are much more metallic in character than the corresponding MOs in the C₄-containing species (LS) [**12-H**]²⁺ (38% and 42% vs 26% and 21%, respectively). Equally, the computed metal spin density is larger in (HS) [**7-H**]²⁺ than in (HS) [**12-H**]²⁺ (0.49 vs 0.39). Presumably the greater metallic contribution to the frontier orbitals of [**7-H**]²⁺ stabilizes the triplet state and

gives rise to the additional degree of metal-centered diradical character in this species when compared with compounds such as **12-H**.

As noted above, di-iron poly-yne-diyl species, which also offer frontier orbitals with appreciable metallic character, have closely lying singlet and triplet states, both of which are populated at ambient temperatures. Perhaps unsurprisingly, the triplet state of the heterobimetallic Ru/Fe model [{Cp(dHpe)Ru}(C₂){Fe(dHpe)Cp}]²⁺ (**8-H**)²⁺, in which the HOMO and LUMO are even more heavily weighted on the metal atoms, 49% and 46%, respectively, is calculated to be 20 kJ/mol more stable than the singlet state. In the triplet state, the metallic spin densities are 0.49 and 0.79 electron on Ru and Fe atoms, respectively. To further test these relationships between the nature of the metal and the length of the carbon chain on the magnetic characteristics of the complexes, we have also considered the heavier heterobimetallic model [{Cp(dHpe)Ru}(C₂){Os(dHpe)Cp}]²⁺, (**9-H**)²⁺. The triplet state in (**9-H**)²⁺ is favored over the singlet state by only 2 kJ/mol in this heterobimetallic system [$\alpha = 85^\circ$ (HS) and 179° (LS)], and again there is significant metallic character in the HOMO and LUMO (44% and 43%, respectively) and large atomic spin densities located on Ru and Os (0.49 and 0.51, respectively).

In summary, our theoretical results predict an open-shell configuration for (**8-H**)²⁺, whereas for [**7-H**]²⁺ and (**9-H**)²⁺ a singlet–triplet equilibrium is expected. In general it seems that triplet states are favored within the family of yne-diyl- and poly-yne-diyl-bridged bimetallic complexes by the presence of iron centers or of shorter carbon chains. The longer bridges and heavier metal components promote greater stability of the closed-shell singlet states. These factors are almost balanced in the ruthenium- and osmium-containing examples [**7-H**]²⁺ and (**9-H**)²⁺, and the singlet and triplet states are energetically almost equivalent.

In addition to the electronic factors described above, steric hindrance between the bulky dppe ligands would be expected to influence the relative stability of the conformers of complex **7**, while solvation and ion-pairing effects could also be anticipated to become significant additional factors in electrolyte solutions. To investigate the role steric effects may play in the conformational stability of ruthenium ethynediyl complexes, geometry optimizations (QM/MM) followed by full DFT single-point calculations were performed on [**7**]ⁿ⁺ ($n = 0, 2$) (see computational details). An energy minimum is found for a C(0)···Ru···C(0) torsion angle of 61° for **7**, very close to the value of 59.3° determined crystallographically. For the LS dicationic species [**7**]²⁺, the *transoid* form is calculated to be 28 kJ/mol higher in energy than the most stable arrangement, which is computed for $\alpha = 55^\circ$ (angles of 52.6° and 60.8° are experimentally measured). Significant steric effects hampered efforts to calculate sensible energies of the *cisoid* forms ($\alpha = 0^\circ$). Therefore, conformations of [**7**]ⁿ⁺ in both solution and in the solid state are likely to be strongly influenced by steric interactions between the bulky dppe ligands. Indeed, on the basis of these calculations the steric effects are likely the predominant interaction and easily able to overcome the much smaller electronic energetic factors described above for the [**7-H**]ⁿ⁺ series. However, it is noteworthy that QM/MM-DFT calculations performed on [**7**]²⁺ show that the ferromagnetic triplet state is 3 kJ/mol lower in energy than the antiferromagnetic singlet state (broken symmetry calculation).

Magnetism. Solutions of the dications give broad NMR spectra, which sharpen somewhat upon cooling the solutions and suggest a degree of paramagnetism. This has been confirmed

(37) Jiao, H.; Costuas, K.; Gladysz, J. A.; Halet, J.-F.; Guillelot, M.; Toupet, L.; Paul, F.; Lapinte, C. *J. Am. Chem. Soc.* **2003**, *125*, 9511.

Table 2. Electrochemical Data for the C₂ Complexes Reported Here and Related Compounds

complex	E ₁ ^a	E ₂ ^a	E ₃	E ₄	ΔE°
7	-0.61	+0.21	+1.06	+1.74 ^b	820/850/680
8	-0.75	+0.16	+1.04		910/880
9	-0.67	+0.09	+1.00		760/910
10	-0.60	+0.22	+1.07		820/850
11	-0.78	+0.04	+0.95		820/910
Mn–Mn ^c	-2.364	-1.375	-0.387		988/988
13	-0.24	+0.35	+1.08	+1.44 ^b	0.59/

^a Potentials in V vs FeCp₂[FeCp₂]⁺ (+0.46 V) from CH₂Cl₂ solutions containing 0.1 M NBu₄PF₆ supporting electrolyte. ^b Irreversible. ^c Data from NCMe/NBu₄PF₆ solutions and converted assuming FeCp₂[FeCp₂]⁺ = 0.40 V.

in the case of [7](PF₆)₂ by measurements of the magnetic susceptibilities of solid samples over the temperature range 4–300 K. The room-temperature moment of 0.46 μ_B remains constant between 300 and 100 K, then decreases gradually to reach 0.3 μ_B at 4 K. The corresponding χ_M data follow a Curie temperature dependence. These values are very small and close to being diamagnetic after allowing for the diamagnetic corrections of the ligands. Susceptibilities are bulk measurements that indicate the presence of weak paramagnetism, but they cannot specify if unpaired electron spins are or are not localized on the Ru or C₂ fragments.

Small paramagnetic susceptibilities can, of course, originate from a variety of sources, a possible one being the presence of paramagnetic impurities in an otherwise diamagnetic material. In principle, they can originate from second-order Zeeman effects on the Ru centers, but these would be expected to be independent of temperature, which is not the case in the present example. Of particular relevance to the present and related μ-C₂ species is the occurrence of spin-triplet as well as spin-singlet states (*vide infra*). What is clear is that the present μ_{eff} values are much smaller than those reported for the related μ-C₂-manganese complexes [{Cp'(dmpe)Mn}–CC–{Mn(dmpe)Cp'}]ⁿ⁺, where n = 0 or 1,²³ the former having a value of 2.47 μ_B at room temperature, which decreased to 2.28 μ_B at 2 K, and ascribed to population of a spin-triplet state at all temperatures, which should lead to a μ_{eff} value of 2.8 μ_B. The authors proposed a spin-triplet/singlet equilibrium with S = 1 close in energy above S = 0 to explain the temperature dependence in μ_{eff}. The n = 1 cation showed a most unusual increase in μ_{eff} from 0.69 μ_B at 300 K to 1.67 μ_B at 5 K, and this was ascribed to one unpaired spin. An alternative possibility is that ferromagnetic coupling of two spins is occurring in that case combined with a spin-triplet/singlet equilibrium. Returning to the results obtained for the present dication, the data could be indicative of a triplet/singlet equilibrium with the S = 1 state at energy ≫kT above the ground S = 0 state. However, since μ_{eff} does not approach zero at intermediate temperatures, because of the population of the singlet state, it is more likely that a mixture of singlet- and triplet-state molecules exists in these solid samples with the singlet being dominant.

Electrochemical and Spectro-electrochemical Studies.

Table 2 contains details of the electrochemical responses of the various homo- and heterometallic complexes described herein, together with data for the Mn₂C₂ complexes described by Berke et al.²³ For **7**, four waves are found corresponding to three reversible and one irreversible 1-e processes. The low value for E¹ (–0.61 V) is consistent with the observed ready oxidation of the neutral complex to the monocation, which in turn is also easily oxidized (E² = +0.21 V) to the dication. Two further 1-e events found at +1.06 and +1.74 V have not been realized in chemical processes to date. Most notable are the large ΔE°

values found in the C₂ system (between 820 and 850 mV), which are indicative of the thermodynamic stability of the intermediate oxidation states. It should be emphasized that these electrochemical data alone do not provide unambiguous evidence for, nor do they quantify, electronic interactions between the metal centers.³⁸

The ability of **7** to be oxidized easily can be qualitatively rationalized by the nature and energies of the HOMOs calculated for **7-H**. The two highest occupied orbitals lie at rather high energy and are well separated from the LUMOs (the HOMO/LUMO energy gap is 1.39 eV) and the rest of the occupied MOs (by 1.19 eV). Therefore **7** should be capable of losing up to four electrons to give a series of five oxidation states, as observed. Curiously, the oxidation potentials of **7** and **10** vary little, despite the introduction of the more electron-donating Cp* group in **10**. Only the first oxidation in the heterometallic complexes **9** and **11** displays any significant variation as a function of the supporting ligands. Arguably, more pronounced changes are observed as a function of the metal center, and substitution of a ruthenium center in **7** by either iron (as in **8**) or osmium (as in **9** or **11**) renders the latter complexes generally more prone to oxidation.

Although there are few directly comparable examples of buta-1,3-diyndiyl complexes with the combination of metal end-caps reported here, some comparison is possible between **7** and the complex {Ru(dppe)Cp}₂(μ-C≡CC≡C) (**12**), which also permits comparison of the effects of chain length in these shortest members of the “all-carbon” bridging ligand family.³⁹ The first two oxidation events from the C₂ complex **7** are at markedly lower potentials than are found for the C₄ analogue **12**. As noted above, although the nature and nodal properties of the HOMOs do not change significantly upon lengthening of the carbon chain, they are less heavily weighted toward the metal centers as the chain is lengthened.⁴⁰ This results in a weaker antibonding interaction between the metals and the carbon bridge, and consequently the HOMO energies are lowered when the length of the carbon chain increases (–3.07 eV in **12-H** vs –2.93 eV in **7**, for instance). Similar observations have been reported in the Re(NO)(PPh₃)Cp* series.⁴¹ Curiously, the third oxidation potential occurs at virtually the same potential in both **7** and **12**, while the fourth oxidation is actually *more* thermodynamically favorable in the case of the longer chain complex.

The high thermodynamic stabilities of the various electrochemically detected species prompted an investigation of their electronic spectra by spectro-electrochemical means (Figure 3, Table 3). The electronic spectrum of the monocation [7]⁺ (observed by electrochemical reduction of the isolable dication [7]²⁺ in an OTTLE cell at –30 °C) is dominated by a broad band near 14 500 cm^{–1}. The NIR spectra of ligand-bridged bimetallic complexes {ML_n}(μ-bridge){ML_n} with odd-electron counts have been the subject of considerable discussion, with most authors favoring an interpretation based on the theories of Hush and others.⁴² However, the Hush model assumes that the redox processes are metal-centered. In the present case, the significant involvement of the ethynediyl moiety in the redox-active orbitals suggests a more cautious approach should be

(38) (a) Maurer, J.; Winter, R. F.; Sarkar, B.; Fiedler, J.; Zalis, S. *Chem. Commun.* **2004**, 1900. (b) Barriere, F.; Geiger, W. E. *J. Am. Chem. Soc.* **2006**, *128*, 3980.

(39) Bruce, M. I.; Ellis, B. G.; Gaudio, M.; Lapinte, C.; Melino, G.; Paul, F.; Skelton, B. W.; Smith, M. E.; Toupet, L.; White, A. H. *Dalton Trans.* **2004**, 1601.

(40) Coat, F.; Paul, F.; Lapinte, C.; Toupet, L.; Costuas, K.; Halet, J.-F. *J. Organomet. Chem.* **2003**, *683*, 368.

(41) Dembinski, R.; Bartik, T.; Bartik, B.; Jaeger, M.; Gladysz, J. A. *J. Am. Chem. Soc.* **2000**, *122*, 810.

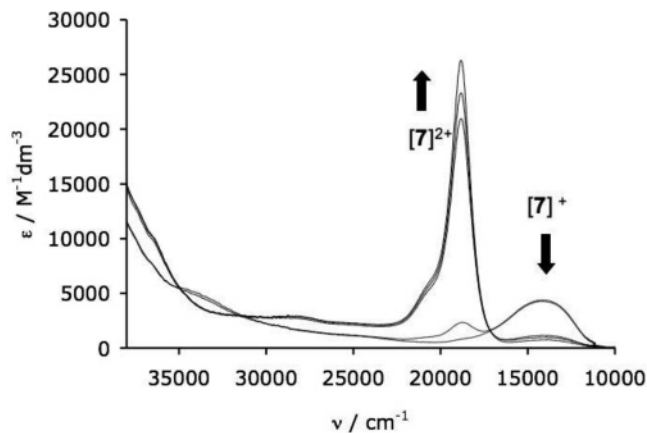


Figure 3. Spectroelectrochemically generated UV-vis-NIR spectroscopic profiles of $[7]^+$ and $[7]^{2+}$ showing their interconversion.

Table 3. Principal Electronic Transition Energies and Intensities from the UV-Vis-NIR Spectra of 7^{n+} ($n = 1-3$), Determined Spectro-electrochemically

	$\bar{\nu}_{\max}$ (cm ⁻¹)/ ϵ (M ⁻¹ dm ⁻³)
7^+	14 150/4400
	34 000/5000
7^{2+}	18 900/26 000
	20 750/5500
	28 000/2800
7^{3+}	18 970/20 200
	25 500/9700

taken. To aid the interpretation of the NIR spectrum of $[7]^+$, we have again turned to DFT computations.

Time-dependent density functional theory (TD-DFT) was used to calculate the first vertical electronic transition energies for the monocationic model $[7\text{-H}]^+$ with its most stable conformation ($\alpha = 55^\circ$) and also with the *transoid* arrangement. The lowest energy excitation of any significant oscillator strength was found in both conformations at 16 200 cm⁻¹ (oscillator strength $f = 0.17$). This excitation, energetically isolated from other absorptions, comprises electronic transitions from the highest occupied spin-orbital HOSO-1 (β) to the lowest unoccupied spin-orbital (LUSO) (β) (70%), and from the HOSO-3 (β) to the LUSO (β) (13%). Interestingly, the LUSO is equally distributed on the metal atoms and the C₂ chain. This low-energy excitation can be described as a Ru(d)-[Ru(d)/C₂(π)]* transition rather than an intervalence charge transfer (IVCT) transition. In addition, two excitations some 10 times weaker are computed at 15 550 and 14 655 cm⁻¹ for the *transoid* conformer. These lower energy excitations involve HOSO (α) (Ru_d-C₂(π) character) to LUSO (α) (Ru-dHpe antibonding character) and HOSO-3 (β) (Ru_d) to LUSO (β) (Ru_d-C₂(π) character) transitions, respectively.

An intense band at 18 900 cm⁻¹ develops upon oxidation of the monocation $[7]^+$, with concomitant collapse of the lower energy feature associated with the monocation. Clean interconversion of the mono- and dication is evidenced by the isosbestic point near 17 200 cm⁻¹. The new band is identical to that observed for the chemically formed and isolated dication. The profile of this band is virtually identical to that observed for the analogous C₄ complex $\{[\text{Ru}(\text{dppe})\text{Cp}]_2(\mu\text{-C}_4)\}^{2+}$, but it is

found at somewhat lower energy. An electronic excitation is computed at 17 900 cm⁻¹ ($f = 0.25$) and at 18 240 cm⁻¹ ($f = 0.18$) for the dicationic models (LS) and (HS) $[7\text{-H}]^{2+}$, respectively. For both models, this relatively high-intensity band is assigned to an electronic transition between an Ru(d)-ligand-based orbital and an [Ru(d)/C₂(π)]*-based orbital.

Oxidation to the trication $[7]^{3+}$ was also achieved. The spectral profile of $[7]^{3+}$ is, again not surprisingly, similar to that of the related C₄ species, but the shift in the visible band is less pronounced. However, the decrease in band intensity and small shift in the band maximum are obvious (Table 3). Further oxidation to the electrochemically detected 32-electron tetracationic species $[7]^{4+}$ was complicated by the chemical reactivity of this species, with rapid decomposition of the sample in solution being evidenced by the accompanying irreversible loss of spectroscopic features.

Conclusions

Several novel complexes in which C₂ groups are end-capped by redox-active group 8 metal centers have been prepared. These complexes show three or four successive 1-e oxidation processes. The redox-related series of complexes $[\text{Ru}(\text{dppe})\text{Cp}]_2(\mu\text{-C}_2)[\text{PF}_6]_n$ ($n = 0-2$) have been prepared by chemical methods and crystallographically characterized. The structural data, together with theoretical calculations, show a gradual progression from an ethynediyl (M-C≡C-M) form in the neutral (36-e) species toward a cumulenic structure (M=C=C=M) in the 34-e dication as oxidation proceeds. A low-energy band in the monocation is observed and on the basis of DFT calculations is assigned to an Ru(d)-[Ru(d)/C₂(π)]* transition. Computational studies indicate a larger metallic character in the frontier orbitals of these dicarbon species relative to their buta-1,3-diyne diyl analogues. Consequently the dicarbon-bridged 34-electron dimetallacumulene dication exhibits paramagnetic and diamagnetic states of comparable energy, in a situation that is analogous to 34-electron iron-based buta-1,3-diyne diyl species. In general, shorter chains and lighter metals lead to increased stability of the triplet states in carbon-bridged bimetallic complexes of group 8.

Experimental Section

General Procedures. All reactions were carried out under dry nitrogen, although normally no special precautions to exclude air were taken during subsequent workup. Common solvents were dried, distilled under argon, and degassed before use.

Instruments. IR spectra were obtained on a Bruker IFS28 FT-IR spectrometer. Spectra in CH₂Cl₂ were obtained using a 0.5 mm path-length solution cell with NaCl windows. Nujol mull spectra were obtained from samples mounted between NaCl discs. NMR spectra were recorded on a Varian 2000 instrument (¹H at 300.13 MHz, ¹³C at 75.47 MHz, ³¹P at 121.503 MHz). Unless otherwise stated, samples were dissolved in CDCl₃ contained in 5 mm sample tubes. Chemical shifts are given in ppm relative to internal tetramethylsilane for ¹H and ¹³C NMR spectra and external H₃PO₄ for ³¹P NMR spectra. UV-vis spectra were recorded on a Varian Cary 5 UV-vis/NIR spectrometer. Electrospray mass spectra (ES-MS) were obtained from samples dissolved in MeOH unless otherwise indicated. Solutions were injected into a Varian Platform II spectrometer via a 10 mL injection loop. Nitrogen was used as the drying and nebulizing gas. Chemical aids to ionization were used.⁴³ Cyclic voltammograms were recorded from CH₂Cl₂ solutions

(42) (a) Hush, N. S. *Prog. Inorg. Chem.* **1967**, *8*, 391. (b) Creutz, C. *Prog. Inorg. Chem.* **1983**, *30*, 1. (c) Brunshwig, B. S.; Creutz, C.; Sutin, N. *Chem. Soc. Rev.* **2002**, *31*, 168. (d) Crutchley R. J. *Adv. Inorg. Chem.* **1994**, *41*, 273. (e) Demadis, K. D.; Hartshorn, C. M.; Meyer, T. J. *Chem. Rev.* **2001**, *101*, 2655.

(43) Henderson, W.; McIndoe, J. S.; Nicholson, B. K.; Dyson, P. J. *J. Chem. Soc., Dalton Trans.* **1998**, 519.

containing 0.1 M $[\text{NBu}_4]\text{PF}_6$ as supporting electrolyte using a PAR model 263 apparatus, with ferrocene as internal calibrant ($\text{FeCp}_2/[\text{FeCp}_2]^+ = 0.46 \text{ V}$). The OTTLE cell has been described elsewhere⁴⁴ and featured a 1 mm path-length cell with a Pt-mesh working electrode and Pt wire counter and pseudo-reference electrodes. Samples (1 mM) were dissolved in CH_2Cl_2 containing 0.5 M $[\text{NBu}_4]\text{BF}_4$ as the supporting electrolyte for the spectroelectrochemical experiments. Elemental analyses were performed by CMAS, Belmont, Vic., Australia. The magnetic susceptibilities were measured using a Quantum Design MPMS5 Squid magnetometer, in an applied field of 1 T, with the sample contained in a quartz tube carefully sealed to prevent any sample decomposition. Freshly prepared samples gave reproducible data.

Reagents. The complexes $\text{MCl}(\text{dppe})\text{Cp}'$ ($\text{Cp}' = \text{Cp}$, $\text{M} = \text{Fe}$,⁴⁵ Ru ,⁴⁶ Os ;⁴⁷ $\text{Cp}' = \text{Cp}^*$, $\text{M} = \text{Ru}$,^{27b} Os ;⁴⁷), $\text{HC}\equiv\text{CSiMe}_3$,⁴⁸ and $[\text{Ru}(\text{C}=\text{CH}_2)(\text{dppe})\text{Cp}^*]\text{PF}_6$ ^{27b} were prepared by the cited methods.

(a) $[\text{Fe}(\text{C}=\text{CH}_2)(\text{dppe})\text{Cp}]\text{PF}_6$ (1). A solution of $\text{FeCl}(\text{dppe})\text{Cp}$ (500 mg, 0.90 mmol), $[\text{NH}_4]\text{PF}_6$ (294 mg, 1.80 mmol), and $\text{HC}\equiv\text{CSiMe}_3$ (0.64 mL, 4.50 mmol) in *t*-BuOH (10 mL) was heated at reflux point for 2 h. The resulting precipitate was collected by filtration and washed with Et_2O to yield $[\text{Fe}(\text{C}=\text{CH}_2)(\text{dppe})\text{Cp}]\text{PF}_6$ (1) (559 mg, 90%). IR (Nujol, cm^{-1}): $\nu(\text{CC})$ 1626w, $\nu(\text{PF})$ 842s. ^1H NMR (d_6 -acetone): δ 3.06–3.37 (m, 4H, CH_2CH_2), 3.99 (s, 2H, CCH_2), 5.25 (s, 5H, Cp), 7.42–7.73 (m, 20H, Ph). ^{13}C NMR (d_6 -acetone): δ 90.15 (s, Cp), 106.93 (s, C_β), 129.42–137.47 (m, Ph), 354.71 [t, $^2J(\text{CP}) = 33 \text{ Hz}$, C_α]. ^{31}P NMR (d_6 -acetone): δ 98.0 (s, dppe); -142.5 [septet, $^1J(\text{PF}) = 703 \text{ Hz}$, PF_6]. ES-MS (positive ion mode, MeOH, m/z): 545, $[\text{Fe}(\text{CCH}_2)(\text{dppe})\text{Cp}]^+$; 519, $[\text{Fe}(\text{dppe})\text{Cp}]^+$.

(b) $[\text{Ru}(\text{C}=\text{CH}_2)(\text{dppe})\text{Cp}]\text{PF}_6$ (2). Similarly, $\text{RuCl}(\text{dppe})\text{Cp}$ (500 mg, 0.83 mmol), $[\text{NH}_4]\text{PF}_6$ (272 mg, 1.67 mmol), and $\text{HC}\equiv\text{CSiMe}_3$ (0.59 mL, 4.15 mmol) in *t*-BuOH (10 mL) gave $[\text{Ru}(\text{C}=\text{CH}_2)(\text{dppe})\text{Cp}]\text{PF}_6$ (2) (554 mg, 91%). IR (Nujol): $\nu(\text{CC})$ 1640w, $\nu(\text{PF})$ 839s. ^1H NMR (d_6 -acetone): δ 3.08–3.24 (m, 4H, CH_2CH_2), 3.20 [t, $^4J(\text{HP}) = 1.5 \text{ Hz}$, 2H, CCH_2], 5.65 (s, 5H, Cp), 7.34–7.83 (m, 20H, Ph). ^{31}P NMR (d_6 -acetone): δ 80.8 (s, dppe); -142.4 [septet, $^1J(\text{PF}) = 703 \text{ Hz}$, PF_6]. Lit. values:²⁵ IR (Nujol): $\nu(\text{CC})$ 1641w, $\nu(\text{PF})$ 841 s (PF_6). ^1H NMR (CD_2Cl_2): δ 2.95 (m, 4H, CH_2CH_2), 3.19 [t, $^4J(\text{HP}) = 1.5 \text{ Hz}$, 2H, CCH_2], 5.37 (s, 5H, Cp), 7.57–7.16 (m, 20H, Ph).

(c) $[\text{Os}(\text{C}=\text{CH}_2)(\text{dppe})\text{Cp}]\text{PF}_6$ (3). A solution of $\text{OsCl}(\text{dppe})\text{Cp}$ (100 mg, 0.145 mmol), $[\text{NH}_4]\text{PF}_6$ (48 mg, 0.29 mmol), and $\text{HC}\equiv\text{CSiMe}_3$ (0.1 mL, 0.725 mmol) in *t*-BuOH (2.5 mL) was heated at reflux point for 4 h. After removal of solvent under vacuum, the residue was dissolved in a minimum amount of CH_2Cl_2 and filtered into Et_2O . The resulting precipitate was collected to yield $[\text{Os}(\text{C}=\text{CH}_2)(\text{dppe})\text{Cp}]\text{PF}_6$ (3) (40 mg, 56%). IR (Nujol, cm^{-1}): $\nu(\text{CC})$ 1641w, $\nu(\text{PF})$ 837s. ^1H NMR (d_6 -acetone): δ 0.62 (t, $^4J_{\text{HP}} = 0.23 \text{ Hz}$, 2H, CCH_2), 3.22–2.94 (m, 4H, CH_2CH_2), 5.76 (s, 5H, Cp), 7.91–7.14 (m, 20H, Ph). ^{13}C NMR (d_6 -acetone): δ 90.79 (s, Cp), 95.06 (s, C_β), 126.73–139.29 (m, Ph), 302.91 (s, C_α). ^{31}P NMR (d_6 -acetone): δ 42.9 (s, dppe); -141.6 (septet, $^1J_{\text{PF}} = 703 \text{ Hz}$, PF_6). ES-MS (positive ion mode, MeOH, m/z): 681, $[\text{Os}(\text{CCH}_2)(\text{dppe})\text{Cp}]^+$; 655, $[\text{Os}(\text{dppe})\text{Cp}]^+$. The filtrate was then purified by chromatography (silica gel), eluting with acetone/hexane (3:7) to recover unreacted $\text{OsCl}(\text{dppe})\text{Cp}$ (40 mg, 40%).

(d) $[\text{Os}(\text{C}=\text{CH}_2)(\text{dppe})\text{Cp}^*]\text{PF}_6$ (4). Similarly, $\text{OsCl}(\text{dppe})\text{Cp}^*$ (160 mg, 0.211 mmol), $[\text{NH}_4]\text{PF}_6$ (69 mg, 0.422 mmol), and $\text{HC}\equiv\text{CSiMe}_3$ (0.14 mL, 1.054 mmol) in MeOH (15 mL) were heated at reflux point for 3 h, subsequent workup giving

$[\text{Os}(\text{C}=\text{CH}_2)(\text{dppe})\text{Cp}^*]\text{PF}_6$ (4) (160 mg, 85%). IR (Nujol, cm^{-1}): $\nu(\text{CC})$ 1633w, $\nu(\text{PF})$ 836s. ^1H NMR (d_6 -acetone): δ 0.60 (s, 2H, CCH_2), 1.74 (s, 15H, Cp^*), 2.86–3.06 (m, 4H, CH_2CH_2), 7.24–7.63 (m, 20H, Ph). ^{31}P NMR (d_6 -acetone): δ 40.8 (s, dppe); -142.5 [septet, $^1J(\text{PF}) = 703 \text{ Hz}$, PF_6].

$[\{\text{Ru}(\text{dppe})\text{Cp}\}_2(\mu\text{-CCH})]\text{PF}_6$ (5). Solution A: AgOTf (144 mg, 0.56 mmol) was added to a solution of $\text{RuCl}(\text{dppe})\text{Cp}$ (350 mg, 0.58 mmol) in thf (20 mL), and the suspension was stirred in the dark for 30 min.

Solution B: In a separate flask, $[\text{Ru}(\text{C}=\text{CH}_2)(\text{dppe})\text{Cp}]\text{PF}_6$ (429 mg, 0.583 mmol) was treated with LiBu (0.48 mL of a 2.5 M solution in hexanes, 1.22 mmol), and the resulting solution was stirred at rt for 30 min.

Solution A was filtered through a pad of Celite into solution B. Stirring was continued at rt for 12 h. The orange solution was then passed through a short silica column, completing the elution with acetone to give a green product. After removal of solvent, the residue was extracted into a minimum amount of CH_2Cl_2 and filtered into rapidly stirred Et_2O (300 mL) to give $[\{\text{Ru}(\text{dppe})\text{Cp}\}_2(\mu\text{-CCH})]\text{PF}_6$ (5) (508 mg, 70%) as a forest-green powder. An analytical sample was recrystallized from CH_2Cl_2 /hexane. Anal. Calcd ($\text{C}_{64}\text{H}_{59}\text{F}_6\text{P}_5\text{Ru}_2$): C, 59.17; H, 4.57; M (cation), 1154. Found: C, 59.30; H, 4.53. IR (Nujol, cm^{-1}): 1651m, 837s. ^1H NMR (CD_2Cl_2): δ 1.91, 2.08 (2 \times m, 2 \times 4H, CH_2), 2.51 [qu, $J(\text{HP}) = 6 \text{ Hz}$, $\text{C}=\text{CH}$], 4.75 (s, 10H, Cp), 6.52–8.02 (m, 40H, Ph). ^{31}P (CD_2Cl_2): δ 81.7 (s, dppe), -142.4 (septet, PF_6). ES-MS (MeOH, m/z): 1154, M^+ ; 577, M^{2+} .

(e) $[\{\text{Cp}(\text{dppe})\text{Ru}\}_2(\mu\text{-C}_2)]\text{PF}_6$ (7) $(\text{PF}_6)_2$. $[\text{FeCp}_2]\text{PF}_6$ (38 mg, 0.115 mmol) was added to a solution of $[\{\text{Cp}(\text{dppe})\text{Ru}\}_2(\mu\text{-CCH})]\text{PF}_6$ (150 mg, 0.115 mmol) in CH_2Cl_2 (15 mL), and the mixture was stirred for 30 min. Solvent was then removed under vacuum, and the residue was dissolved in a minimum amount of benzene and chromatographed (silica gel), eluting with acetone/hexane (1:9) to remove FeCp_2 and then acetone/hexane (3:7) to yield $[\{\text{Cp}(\text{dppe})\text{Ru}\}_2(\mu\text{-C}_2)]\text{PF}_6$ (7) $(\text{PF}_6)_2$ (137 mg, 92%). Anal. Calcd ($\text{C}_{64}\text{H}_{58}\text{F}_6\text{P}_5\text{Ru}_2$): C, 59.21; H, 4.50; M (cation), 1154. Found: C, 59.30; H, 4.53. IR (Nujol, cm^{-1}): $\nu(\text{CC})$ 1713w, $\nu(\text{PF})$ 839s. ES-MS (positive ion mode, MeOH, m/z): 1154, M^+ .

(f) $[\{\text{Cp}(\text{dppe})\text{Ru}\}_2(\mu\text{-C}_2)](\text{PF}_6)_2$ (7) $(\text{PF}_6)_2$. $[\text{FeCp}_2]\text{PF}_6$ (76 mg, 0.23 mmol) was added to a solution of $[\{\text{Cp}(\text{dppe})\text{Ru}\}_2(\mu\text{-CCH})]\text{PF}_6$ (150 mg, 0.115 mmol) in CH_2Cl_2 (15 mL) and stirred for 30 min. The solvent was then removed under vacuum, and the residue dissolved in a minimum amount of benzene and chromatographed (silica gel), eluting with acetone/hexane (1:9) to remove FeCp_2 and then acetone/hexane (1:1) to yield $[\{\text{Cp}(\text{dppe})\text{Ru}\}_2(\mu\text{-C}_2)](\text{PF}_6)_2$ (7) $(\text{PF}_6)_2$ (166 mg, 89%). Anal. Calcd ($\text{C}_{64}\text{H}_{58}\text{F}_{12}\text{P}_6\text{Ru}_2$): C, 53.18; H, 4.05; M (dication), 577. Found: C, 53.09; H, 4.07. IR (Nujol, cm^{-1}): $\nu(\text{CC})$ 1651w, $\nu(\text{PF})$ 840s. ES-MS (positive ion mode, MeOH, m/z): 577, $[\text{M}]^{2+}$.

$[\{\text{Cp}(\text{dppe})\text{Ru}\}_2(\mu\text{-C}\equiv\text{C})]$ (7). KOBu^t (35 mg, 0.31 mmol) was added to a suspension of $[\{\text{Ru}(\text{dppe})\text{Cp}\}_2(\mu\text{-CCH})]\text{PF}_6$ (100 mg, 0.08 mmol) in thf (5 mL). The color changed rapidly from green to orange, and after ca. 5 min, hexane (50 mL) was added. Concentration to 20 mL and addition of CH_2Cl_2 (1 mL) gave an orange solution, which was left to crystallize under a gentle stream of N_2 . After 24 h, red crystals had separated. These were collected and washed with acetone and dry Et_2O to give $[\{\text{Cp}(\text{dppe})\text{Ru}\}_2(\mu\text{-C}\equiv\text{C})]$ (7) (24 mg, 27%). Anal. Calcd ($\text{C}_{64}\text{H}_{58}\text{P}_4\text{Ru}_2$): C, 66.66; H, 5.07; M, 1153. Found: C, 66.70; H, 5.06. IR (Nujol, cm^{-1}): 1951m. ^1H NMR (C_6D_6): δ 1.92, 2.11 (2 \times m, 2 \times 4H, CH_2), 4.59 (s, 10H, Cp), 6.85–7.93 (m, 40H, Ph). ^{13}C NMR (C_6D_6): δ 29.09 (m, CH_2), 82.84 (s, Cp), 129.18–145.90 (m, Ph). ^{31}P NMR (C_6D_6): δ 87.8 (br). ES-MS (positive ion, MeOH, m/z): 1154, $[\text{M}]^+$; 577, $[\text{M} + \text{H}]^{2+}$.

$[\{\text{Cp}(\text{dppe})\text{Ru}\}_2\text{C}\equiv\text{C}\{\text{Ru}(\text{dppe})\text{Cp}^*\}]$ (10). To a solution of $[\{\text{Cp}(\text{dppe})\text{Ru}\}_2\text{CC}\{\text{Ru}(\text{dppe})\text{Cp}^*\}]\text{PF}_6$ (100 mg, 0.066 mmol) in THF (10 mL) was added an excess of KOBu^t (23 mg, 0.198

(44) Duff, C. M.; Heath, G. A. *Inorg. Chem.* **1991**, *30*, 2528.

(45) Mays, M. J.; Sears, P. L. *J. Chem. Soc., Dalton Trans.* **1973**, 1873.

(46) Gutierrez, A. A.; Ballester Reventos, L. *J. Organomet. Chem.* **1998**, *338*, 249.

(47) Perkins, G. J.; Bruce, M. I.; Skelton, B. W.; White, A. H. *Inorg. Chim. Acta* **2006**, *359*, 2644.

(48) Holmes, A. B.; Sporikou, C. N. *Organic Syntheses*; Wiley: New York, 1993; Collect. Vol. 8, p 606.

Table 4. Crystal Data and Refinement Details

	7	[7]PF ₆	[7](PF ₆) ₂	[7](PF ₆) ₂	[7](PF ₆) ₂
formula	C ₆₄ H ₅₈ F ₄ Ru ₂ ·CH ₂ Cl ₂	C ₆₄ H ₅₈ F ₆ P ₅ Ru ₂	C ₆₄ H ₅₈ F ₁₂ P ₆ Ru ₂	C ₆₄ H ₅₈ F ₁₂ P ₆ Ru ₂ ·C ₃ H ₆ O	C ₆₄ H ₅₈ F ₁₂ P ₆ Ru ₂ ·H ₂ O
MW	1238.14	1298.17	1443.13	1501.21	1461.14
cryst syst	monoclinic	monoclinic	triclinic	triclinic	triclinic
space group	<i>P</i> 2 ₁ / <i>c</i>	<i>P</i> 2 ₁ / <i>n</i>	<i>P</i> $\bar{1}$	<i>P</i> $\bar{1}$	<i>P</i> $\bar{1}$
<i>a</i> /Å	15.210(2)	20.783(10)	11.96(1)	11.538(5)	11.639(2)
<i>b</i> /Å	20.703(2)	12.954(8)	15.49(2)	14.004(6)	15.134(3)
<i>c</i> /Å	19.144(2)	22.97(1)	20.45(2)	21.671(9)	19.865(4)
α /deg			69.70(2)	101.154(7)	69.693(3)
β /deg	111.627(2)	95.480(10)	84.93(2)	91.028(7)	84.767(3)
γ /deg			69.31(2)	112.459(7)	69.351(3)
<i>V</i> /Å ³	5604(1)	6157(6)	3322(6)	3159(2)	3069(1)
ρ_c /g cm ⁻³	1.467	1.40 ₀	1.44 ₃	1.57 ₈	1.58 ₁
<i>Z</i>	4	4	2	2	2
2 θ _{max} /deg	53	50	41	50	55
μ (Mo K α)/mm ⁻¹	0.79	0.68	0.67	0.71	0.73
<i>T</i> _{min} /max	0.90	0.69	0.52	0.80	0.71
cryst dimens/mm ³	0.48 × 0.36 × 0.24	0.13 × 0.05 × 0.04	0.08 × 0.06 × 0.04	0.25 × 0.08 × 0.07	0.54 × 0.27 × 0.16
<i>N</i> _{tot}	48611	41427	25294	28832	14129
<i>N</i> (<i>R</i> _{int})	11347 (0.052)	10951 (0.29)	6797 (0.40)	10911 (0.077)	14129 (0.11)
<i>N</i> _o	9028	3281	1899	7544	8832
<i>R</i>	0.049	0.125	0.16	0.071	0.070
<i>R</i> _w (<i>n</i> _w)	0.067 (0)	0.149 (0)	0.21 (0)	0.18 (<i>wR2</i>)	0.15 (<i>wR2</i>)

mmol), and stirring continued for a further 30 min before the solvent was removed *in vacuo*. The product was then extracted with hot hexane until fractions were colorless, and the solvent was again removed *in vacuo* to yield pure orange {Cp(dppe)Ru}C≡C{Ru(dppe)Cp*} (**10**) (60 mg, 75%). Anal. Calcd (C₆₉H₆₈P₄Ru₂·0.5CH₂Cl₂): C, 65.95; H, 5.49; M, 1224. Found: C, 66.40; H, 5.21. IR (Nujol, cm⁻¹): 2026 m. ¹H NMR (*d*₆-benzene): δ 1.69 (s, 15H, Cp*), 1.98–1.87, 2.15–2.08 (2 × m, 2 × 2H, CH₂CH₂), 4.60 (s, 5H, Cp); 6.76–7.93 (m, 40H, Ph). ¹³C NMR (*d*₆-benzene): δ 10.97 (s, C₅Me₅), 27.69 (m, CH₂CH₂), 83.01 (s, Cp), 92.84 (s, C₅Me₅), 128.07–147.46 (m, Ph). ³¹P NMR (*d*₆-benzene): δ 83.4, 88.7, (br, dppe). ES-MS (positive ion mode, MeOH, *m/z*): 1224, M⁺; 635, [Ru(dppe)Cp*]⁺; 565, [Ru(dppe)Cp]⁺.

{[Cp'(dppe)M](μ -C₂){M(dppe)Cp'}](PF₆)₂. These complexes were prepared by addition of a solution of [M(dppe)Cp']⁺ (solution 1) to one of deprotonated [M(=C=CH₂)(dppe)Cp']⁺ (solution 2). Both solutions were freshly prepared and stirred for 30 min before solution 1 was filtered through Celite into solution 2. The resulting mixture was stirred for a further 18 h and worked up as described below for the individual compounds.

{[Cp(dppe)Ru](μ -C₂){Ru(dppe)Cp*}](PF₆)₂ (**10**)(PF₆)₂. Solution 1: AgOTf (190 mg, 0.741 mmol) was added to RuCl(dppe)Cp (445 mg, 0.741 mmol) in THF (15 mL) in the dark. Solution 2: Bu^tLi (0.6 mL, 1.482 mmol, 2.5 M in hexanes) was added to [Ru(=C=CH₂)(dppe)Cp*]PF₆ (597 mg, 0.741 mmol) in THF (15 mL). After 18 h, the mixture was filtered through a short column of silica gel, eluting with acetone. Solvent was then removed from the green eluate, and the solid was dissolved in CH₂Cl₂ (30 mL). Addition of [FeCp₂]PF₆ (491 mg, 1.48 mmol) turned the solution pink. Chromatography (silica gel), eluting first with acetone/hexane (1:9) to remove unreacted RuCl(dppe)Cp and FeCp₂ and then with acetone/hexane (1:1) gave a pink band containing {[Cp(dppe)Ru](μ -C₂){Ru(dppe)Cp*}](PF₆)₂ (**10**)(PF₆)₂ (426 mg, 38%) and isolated as a pink-colored solid. Anal. Calcd (C₆₉H₆₈F₁₂P₆Ru₂): C, 54.77; H, 4.53; M (dication), 612. Found: C, 54.63; H, 4.51. IR (Nujol, cm⁻¹): ν (CC) 1639w, ν (PF) 841s. ES-MS (positive ion mode, MeOH, *m/z*): 612, M²⁺.

{[Cp(dppe)Fe](μ -C₂){Ru(dppe)Cp}](PF₆)₂ (**8**)(PF₆)₂. Solution 1: AgOTf (19 mg, 0.073 mmol) was added to stirred RuCl(dppe)Cp (44 mg, 0.073 mmol) in THF (10 mL) while in the dark. Solution 2: Bu^tLi (0.06 mL, 0.145 mmol, 2.5 M) was added to [Fe(=C=CH₂)(dppe)Cp](PF₆) (50 mg, 0.073 mmol) in THF (10 mL). After 18 h, chromatography (basic alumina), eluting with acetone, was used to remove the μ -ethynyl complex. The solvent

was then removed, the solid was redissolved in CH₂Cl₂ (10 mL), [FeCp₂]PF₆ (48 mg, 0.146 mmol) was added, and stirring was continued for 30 min before Et₂O (15 mL) was added. The pink precipitate was collected on a sintered glass frit to yield {[Cp(dppe)-Fe](μ -C₂){Ru(dppe)Cp}](PF₆)₂ (**8**)(PF₆)₂ (27 mg, 27%). Anal. Calcd (C₆₄H₅₈F₁₂FeOsP₆): C, 54.99; H, 4.18; M (dication), 554. Found: C, 55.04; H, 4.12. IR (Nujol, cm⁻¹): ν (CC) 1645w, ν (PF) 840s. ES-MS (positive ion mode, MeOH, *m/z*): 554, M²⁺.

{[Cp(dppe)Ru](μ -C₂){Os(dppe)Cp}](PF₆)₂ (**9**)(PF₆)₂. Solution 1: AgOTf (9.5 mg, 0.037 mmol) was added to RuCl(dppe)Cp (22 mg, 0.037 mmol) in THF (10 mL) in the dark. Solution 2: Bu^tLi (0.04 mL, 0.074 mmol, 2.5 M) was added to [Os(=C=CH₂)(dppe)Cp]PF₆ (30 mg, 0.037 mmol) in THF (10 mL). After 18 h, a workup similar to **7** gave {[Cp(dppe)Ru](μ -C₂){Os(dppe)Cp}](PF₆)₂ (**9**)(PF₆)₂ (34 mg, 62%). Anal. Calcd (C₆₄H₅₈F₁₂OsP₆Ru): C, 50.17; H, 3.82; M (dication), 621. Found: C, 49.99; H, 3.88. IR (Nujol, cm⁻¹): ν (CC) 1730w, ν (PF) 844s. ES-MS (positive ion mode, MeOH, *m/z*): 621, M²⁺; 655, [Os(dppe)Cp]⁺; 565, [Ru(dppe)Cp]⁺.

{[Cp(dppe)Ru](μ -C₂){Os(dppe)Cp*}](PF₆)₂ (**11**)(PF₆)₂. Solution 1: AgOTf (190 mg, 0.741 mmol) was added to RuCl(dppe)Cp (445 mg, 0.741 mmol) in THF (15 mL) in the dark. Solution 2: Bu^tLi (0.6 mL, 1.482 mmol, 2.5 M) was added to [Os(=C=CH₂)(dppe)Cp*]PF₆ (663 mg, 0.741 mmol) in THF (15 mL). After 18 h, a similar workup to **10** gave {[Cp(dppe)Ru](μ -C₂){Os(dppe)Cp*}](PF₆)₂ (¹¹(PF₆)₂) (510 mg, 43%). Anal. Calcd (C₆₉H₆₈F₁₂OsP₆Ru): C, 51.72; H, 4.28; M (dication), 656. Found: C, 51.68; H, 4.30. IR (Nujol, cm⁻¹): ν (CC) 1672w, ν (PF) 838s. ES-MS (positive ion mode, MeOH, *m/z*): 656, M²⁺.

Structure Determinations. Full spheres of diffraction data were measured at ca. 153 K using a Bruker AXS CCD area-detector instrument. *N*_{tot} reflections were merged to *N* unique (*R*_{int} cited) after “empirical”/multiscan absorption correction (proprietary software), *N*_o with *F* > 4 σ (*F*) being used in the full matrix least-squares refinements. All data were measured using monochromated Mo K α radiation, λ = 0.71073 Å. Anisotropic displacement parameter forms were refined for the non-hydrogen atoms, (*x*, *y*, *z*, *U*_{iso})_H being constrained at estimates. Conventional residuals *R*, *R*_w on |*F*| are quoted [weights: ($\sigma^2(F) + 0.000n_w F^2$)⁻¹]. Neutral atom complex scattering factors were used; computation used the XTAL 3.7 program system.⁴⁹ Pertinent results are given in Figure 1 (which

(49) Hall, S. R., du Boulay, D. J., Olthof-Hazekamp, R., Eds. *The XTAL 3.7 System*; University of Western Australia, 2000.

shows non-hydrogen atoms with 50% probability amplitude displacement ellipsoids and hydrogen atoms with arbitrary radii of 0.1 Å) and in Tables 1 and 4.

In general, data acquisition and subsequent structure determination presented considerable difficulties as a consequence of specimen size, crystal quality, desolvation, and disorder, with (**7** excepted) generally poor precision incompatible with the aspiration of benchmarking the associated theoretical calculations.

The lattice CH_2Cl_2 of solvation in **7** was modeled as disordered over two sets of sites, occupancies set at 0.5. In $[\text{7}]\text{PF}_6$ and (unsolvated) $[\text{7}](\text{PF}_6)_2$, limited data would support meaningful anisotropic displacement parameter refinement for Ru, P only, aromatic rings being modeled as rigid bodies in the refinement of the latter. The assignment of one compound as a monohydrate rests upon the refinement of a significant isolated residue as a water molecule oxygen atom.

Computational Details. DFT calculations were performed with the Amsterdam Density Functional package (ADF 2004.01)^{50–52} on models $[\text{7-H}]^{n+}$, $[\text{8-H}]^{n+}$, and $[\text{9-H}]^{n+}$, which were used in order to reduce computational effort (phenyl groups of $[\text{7}]^{n+}$, $[\text{8}]^{n+}$, and $[\text{9}]^{n+}$ were replaced by hydrogen atoms). Calculations were also carried out on $[\text{12-H}]^{n+}$ derived from the structure of **12**, for comparison. The geometries were fully optimized without constraints (C_1 symmetry). Electron correlation was treated within the local density approximation (LDA) in the Vosko–Wilk–Nusair parametrization.⁵³ The nonlocal corrections of Becke and Perdew were added to the exchange and correlation energies, respectively.^{54,55} The analytical gradient method implemented by Verluis and Ziegler was used.⁵⁶ The standard ADF TZP basis set was used, i.e., triple- ξ STO basis set for the valence core augmented with a 3d polarization function for C and P and a 5p polarization function for Ru. Orbitals up to 1s, 2p, and 4p were kept frozen for C, P, and Ru, respectively. The gradient-regulated asymptotic correction,⁵⁷ which provides a correct Coulombic asymptotic behavior in the inner atomic region, was used for the TD-DFT excited-state calculations (atomic basis set unchanged). The excitation energies and oscillator strengths were calculated following the procedure described by van Gisbergen and co-workers.⁵⁸ DFT/B3LYP (LanL2DZ basis set) calculations were also performed with the Gaussian 03 program⁵⁹ on $[\text{7-H}]^{2+}$, $[\text{8-H}]^{2+}$, and $[\text{9-H}]^{2+}$ to better evaluate the

spin configuration of those systems since they were shown to give the most reliable results for electronic configurations.⁶⁰ The structural arrangements of $[\text{7}]^{n+}$ ($n = 0–2$) were optimized using the QM/MM methodology implemented in the ADF package. The phenyl groups were described by molecular mechanics (MM) using the SYBYL/TRIPOS 5.2 force field constants. Representations of the molecular structures and orbitals were done using MOLEKEL 4.1.⁶¹

Full details of the structure determinations (except structure factors) have been deposited with the Cambridge Crystallographic Data Centre as CCDC 235746 (**7**), 235747 ($[\text{7}](\text{PF}_6)_2\cdot\text{acetone}$), 613892 ($[\text{7}](\text{PF}_6)_2\cdot 4\text{CH}_2\text{Cl}_2$), 613893 ($[\text{7}]\text{PF}_6$), 613894 ($[\text{7}]\text{PF}_6\cdot\text{H}_2\text{O}$). Copies of this information may be obtained free of charge from The Director, CCDC, 12 Union Road, Cambridge CB2 1EZ, UK (fax: + 44 1223 336 033; e-mail: deposit@ccdc.cam.ac.uk or www: <http://www.ccdc.cam.ac.uk>).

Acknowledgment. We thank Professor Brian Nicholson (University of Waikato, Hamilton, New Zealand) for providing the mass spectra, the ARC for support of this work, and Johnson Matthey plc, Reading, for generous loans of $\text{RuCl}_3\cdot n\text{H}_2\text{O}$ and potassium osmate. K.C. and J.-F.H. thank the Centre Informatique National de l'Enseignement Supérieur (CINES) and the Institut de Développement et de Ressources en Informatique Scientifique (IDRIS-CNRS) for computing facilities. These studies were facilitated by travel grants (ARC, Australia, the Royal Society, UK, and CNRS, France), and an EPSRC Visiting Fellowship (M.I.B./P.J.L.).

Supporting Information Available: Optimized distances and angles computed for the neutral and cationic models of **7-H** are given in Table S1, and a representative cyclic voltammogram of $[\text{7}](\text{PF}_6)_2$ is shown in Figure S1. This material is available free of charge via the Internet at <http://pubs.acs.org>.

OM7002859

(50) te Velde, G.; Bickelhaupt, F. M.; Fonseca Guerra, C.; van Gisbergen, S. J. A.; Baerends, E. J.; Snijders, J. G.; Ziegler, T. *J. Comput. Chem.* **2001**, *22*, 931.

(51) Fonseca Guerra, C.; Snijders, J. G.; te Velde, G.; Baerends, E. J. *Theor. Chem. Acc.* **1998**, *99*, 391.

(52) *ADF2004.01*; Theoretical Chemistry, Vrije Universiteit: Amsterdam, The Netherlands, SCM.

(53) Vosko, S. D.; Wilk, L.; Nusair, M. *Can. J. Chem.* **1990**, *58*, 1200.

(54) Becke, A. D. *Phys. Rev. A* **1988**, *38*, 3098.

(55) Perdew, J. P. *Phys. Rev. B* **1986**, *33*, 8822.

(56) Verluis, L.; Ziegler, T. *J. Chem. Phys.* **1988**, *88*, 322.

(57) Grüning, M.; Gritsenko, O. V.; van Gisbergen, S. J. A.; Baerends, E. J. *J. Chem. Phys.* **2001**, *114*, 652.

(58) van Gisbergen, S. J. A.; Snijders, J. G.; Baerends, E. J. *Comput. Phys. Commun.* **1999**, *118*, 119.

(59) Frisch, M. J.; Trucks, G. W.; Schlegel, H. B.; Scuseria, G. E.; Robb, M. A.; Cheeseman, J. R.; Montgomery, J. A., Jr.; Vreven, T.; Kudin, K. N.; Burant, J. C.; Millam, J. M.; Iyengar, S. S.; Tomasi, J.; Barone, V.; Mennucci, B.; Cossi, M.; Scalmani, G.; Rega, N.; Petersson, G. A.; Nakatsuji, H.; Hada, M.; Ehara, M.; Toyota, K.; Fukuda, R.; Hasegawa, J.; Ishida, M.; Nakajima, T.; Honda, Y.; Kitao, O.; Nakai, H.; Klene, M.; Li, X.; Knox, J. E.; Hratchian, H. P.; Cross, J. B.; Bakken, V.; Adamo, C.; Jaramillo, J.; Gomperts, R.; Stratmann, R. E.; Yazyev, O.; Austin, A. J.; Cammi, R.; Pomelli, C.; Ochterski, J. W.; Ayala, P. Y.; Morokuma, K.; Voth, G. A.; Salvador, P.; Dannenberg, J. J.; Zakrzewski, V. G.; Dapprich, S.; Daniels, A. D.; Strain, M. C.; Farkas, O.; Malick, D. K.; Rabuck, A. D.; Raghavachari, K.; Foresman, J. B.; Ortiz, J. V.; Cui, Q.; Baboul, A. G.; Clifford, S.; Cioslowski, J.; Stefanov, B. B.; Liu, G.; Liashenko, A.; Piskorz, P.; Komaromi, I.; Martin, R. L.; Fox, D. J.; Keith, T.; Al-Laham, M. A.; Peng, C. Y.; Nanayakkara, A.; Challacombe, M.; Gill, P. M. W.; Johnson, B.; Chen, W.; Wong, M. W.; Gonzalez, C.; Pople, J. A. *Gaussian 03*, revision C.02; Gaussian, Inc.: Wallingford, CT, 2004.

(60) Ruiz, E.; Alvarez, S.; Cano, J.; Polo, V. *J. Chem. Phys.* **2005**, *123*, 164110.

(61) Flükiger, P.; Lüthi, H. P.; Portmann, S.; Weber, J. *MOLEKEL 4.1*; Swiss Center for Scientific Computing: Manno, 2000–2001.